ACS APPLIED ENERGY MATERIALS

Forum Article

Cite This: ACS Appl. Energy Mater. 2020, 3, 29−37

www.acsaem.org

CdSe Quantum Dot Sensitized Molecular Photon Upconversion Solar Cells

Drake Beery, Jonathan P. Wheeler, Ashley Arcidiacono, and Kenneth Hanson*

Department of Chemistry & Biochemistry, Florida State University, Tallahassee, Florida 32306, United States

Supporting Information

ABSTRACT: Incorporating photon upconversion, via triplet−triplet annihilation (TTA-UC), directly into a solar cell is an intriguing strategy for harnessing sub-band gap photons and surpassing the Shockley−Queisser limit. A majority of TTA-UC solar cells to date rely on difficult to synthesize and expensive platinum and/or palladium porphyrin sensitizers. Here, we present, as far as we know, the first TTA-UC solar cell that integrates quantum dot (QD) sensitizers directly into the photocurrent generation mechanism. The photoanodes are composed of a nanocrystalline TiO_2 substrate, 4,4′-(anthracene-9,10-diyl)bis(4,1-phenylene)diphosphonic acid (A) as the annihilator molecule, and CdSe QDs as the sensitizer in an inorganic−organic-inorganic layered architecture (TiO_2-A-QD). The TiO_2-A-QD devices generate a photocurrent that is more than 1.4 times the sum of its parts and does so via a TTA-UC mechanism as demonstrated by intensity dependence, IPCE, and spectroscopic measurements. The maximum efficiency onset threshold (i.e., the I_{th} value) of 0.9 mW cm^{-2} (1.9 × 10^{15} ex s^{-1} cm^{-2}) is below solar flux and on par with some of the lowest I_{th} values reported to date. However, the J_{sc} for the QD sensitized device (29 μA cm^{-2}) is still lower than comparable molecular sensitized devices (185 μA cm^{-2}) due in part to lower sensitizer surface loadings, less than unity energy transfer yields (~40−80%), slow regeneration kinetics, and competitive QD* quenching by the $Co^{II/III}(phen)_3$ redox mediator. Nonetheless these results demonstrate that multilayer assemblies containing QD sensitizers is an effective strategy to harness UC in a TTA-UC solar cell.

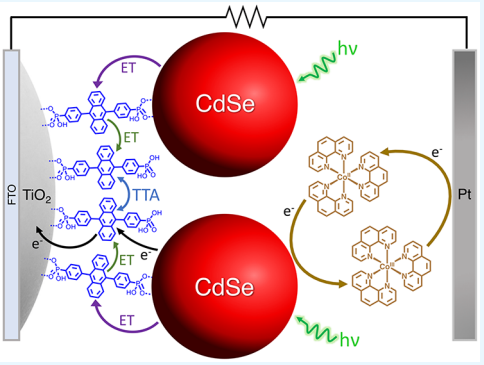

KEYWORDS: *quantum dot, bilayer, triplet−triplet annihilation, photon upconversion, solar energy conversion, energy transfer, solar cell*

1. INTRODUCTION

Photon upconversion by way of triplet−triplet annihilation (TTA-UC) is an intriguing strategy to increase theoretical solar cell efficiencies beyond the Shockley−Queisser limit[1] from ~34% to >43%.[2−4] This efficiency increase is achieved by combining two previously transmitted, sub-band gap, low energy photons into one higher energy excited state that can then be harvested in the solar cell.[5−7] Photocurrent enhancements due to TTA-UC have been demonstrated with both optical (i.e., a standard solar cell combined with a UC filter)[6,8−10] and electronic (i.e., TTA-UC is integrated into the solar cell)[7,11,12] coupling schemes. For the latter, combining TTA-UC sensitizer and acceptor pairs on a metal oxide substrate[13,14] is a popular means of directly extracting charge from the UC state.[12,15] Of the various molecular assembly strategies[16] (e.g., heterogeneous,[12] codeposition,[17] and MOFs,[18]) metal ion linked multilayers[19] have been particularly successful,[15,20,21] recently demonstrating photocurrent enhancements up to 315 μA cm^{-2}.[22] Despite this progress there is much room for improvement in terms of both device optimization and sensitizer−acceptor selection.[7]

Nearly all the integrated TTA-UC solar cells reported to date rely on platinum and/or palladium porphyrin sensitizers. This choice is driven by their well-behaved photophysics, near unity intersystem crossing yields, and previous success in TTA-UC materials.[5,23] However, these porphyrin sensitizers require multistep syntheses, contain rare earth elements, and suffer from inherent energy losses due to the >300 meV S_1-T_1 gap.[24] Recently, quantum dots (QDs) have emerged as an alternative triplet sensitizer that can transfer QD-localized triplet excitons to surface bound or solution organic molecules with near-quantitative efficiency.[25−27] These QD sensitizers have been effectively implemented as the low energy absorber in TTA-UC schemes[28−31] and have even been shown to facilitate TTA-UC and charge separation at a metal oxide interface.[32] In contrast to Pt and Pd porphyrins, QDs are appealing as triplet sensitizers because they are relatively easy to synthesize, contain more earth abundant elements, have small to no S_1-T_1 gap (<15 meV),[33] and their energetics can readily be tuned[34,35]

Special Issue: Young Investigator Forum

Received: September 8, 2019
Accepted: October 30, 2019
Published: November 11, 2019

DOI: 10.1021/acsaem.9b01765
ACS Appl. Energy Mater. 2020, 3, 29−37

to match both the acceptor molecule energetics and the solar spectrum.

Here, we incorporate CdSe QDs as the sensitizer in an integrated TTA-UC solar cell. The photoanode consists of a semiconducting metal oxide, phosphonated acceptor molecules, and CdSe QD sensitizers in a layered inorganic−organic−inorganic architecture as depicted in Figure 1. Device

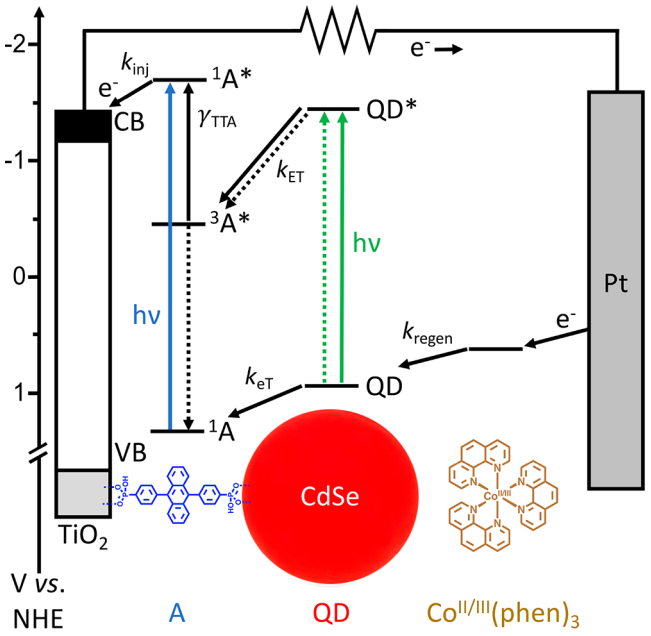

Figure 1. Integrated TTA-UC solar cell architecture with energetics and dynamics, as well as the structure of the molecules studied here (k_{inj} = electron injection, γ_{TTA} = second-order rate constant for TTA, k_{ET} = energy transfer, k_{eT} = electron transfer, and k_{regen} = regeneration rate constants).

measurements indicate that the photocurrent generated from low energy light absorption by the QD is due to a TTA-UC mechanism. Further, spectroscopic techniques were used to show that the device performance is limited by low QD loadings, less than unity energy transfer efficiency, and slow QD regeneration kinetics.

2. EXPERIMENTAL SECTION

2.1. Chemicals. Cadmium oxide (Sigma-Aldrich), oleic acid (Sigma-Aldrich), Se powder (Acros Organics), H_2PtCl_6 (Alfa Aesar), and polyethylene glycol bisphenol A epichlorohydrin copolymer (Sigma-Aldrich) were purchased from their respective suppliers, in parentheses, and used as received. 4,4′-(Anthracene-9,10-diyl)bis(4,1-phenylene)diphosphonic acid (**A**),[36] triphenyl-4,4′-diphosphonic acid (**B**),[37,38] Co^{II}/Co^{III} tris(1,10-phenanthroline),[39] and TiO_2 sol−gel[40] were synthesized according to previous procedures (see the Supporting Information for more details). Octadecene used in QD synthesis was dried and degassed prior to use. All other reagents and solvents (analytical reagent grade) were purchased and used without further purification from Sigma-Aldrich.

2.2. Materials. Oleic acid capped CdSe quantum dots were synthesized according to a previous procedure[41] with three purification cycles of DCM and ethanol washes (see the Supporting Information for more details). The product was obtained through centrifugation, dried under vacuum overnight, and stored under N_2 at 2 °C.

Fluorine-doped tin oxide (FTO)-coated glass (sheet resistance 15 Ω $\square^{-1}$) was purchased from Hartford Glass Co. Meltonix film (1170-25) and the Vac'n Fill Syringe (65209) were purchased from Solaronix. Micro glass cover slides (18 × 18 mm) were obtained from VWR.

2.3. Device Assembly. TiO_2 films were cast using the doctor blade method (3 M Scotch tape) onto a FTO-glass substrate and then sintered in an oven at 500 °C for 15 min.[41] The resulting films were then immersed into an 200 μM solution of **A** or **B** in DMSO for 48 h, then rinsed with methanol, and dried under a stream of air. Next, the films were immersed into an 50 μM solution of CdSe QDs in DCM for 24 h, rinsed with DCM, dried under an N_2 stream, etched to a 1 × 1 cm active area, and used as the anode. The Pt cathode was prepared by drop-casting H_2PtCl_6 solution in ethanol (50 μL, 5 mM) that was heat-dried at 400 °C for 20 min. The films were then sealed together using Melatonix thermoplastic. The sandwiched cells were then transferred to a glovebox where dry and oxygen-free MeCN containing 0.2 M/0.02 M Co^{II}/Co^{III} tris(1,10-phenanthroline) was injected using a Vac'n Fill Syringe (Solaronix), and the solvent injection hole was sealed using thermoplastic and a small glass coverslip.

2.4. Characterization. *2.4.1. Instrumentation.* UV−vis absorption, current density−voltage (*J-V*), incident photon to current efficiency (IPCE), amperometric current−time (*i-t*), intensity dependence, steady-state and time-resolved emission, and transient absorption measurements were performed on previously reported instrumentation (see the Supporting Information for more details).[15,42]

2.4.2. Surface Coverages. Surface coverages (Γ in nmol cm^{-2}) were estimated with the expression $\Gamma = (A(\lambda_{abs})/\varepsilon(\lambda))/1000$,[43] where $A(\lambda)$ is the absorbance of each component on the fully loaded films and ε is the molar extinction coefficient of **A** ($\varepsilon_{397\ nm} = 1.2 \times 10^4\ M^{-1}\ cm^{-1}$) and **QD** (Table S1) in DMSO and DCM, respectively.

3. RESULTS AND DISCUSSION

3.1. Multilayer Assembly. The photoanode used in this study is composed of nanocrystalline TiO_2, 4,4-(anthracene-9,10-diyl)bis(4,1-phenylene) diphosphonic acid (**A**), and cadmium(II) selenide quantum dots (**QD**) as depicted in Figure 1. **A** was selected as the triplet acceptor (a.k.a., emitter, annihilator) because it is our prototype annihilator for our multilayer TTA-UC solar cells[36] and is a derivative of the well-studied 9,10-diphenylanthracene.[5] The geometrically opposed phosphonate groups are critical for binding to both TiO_2[44] and QDs.[41]

Cadmium(II) selenide was selected as the QD of interest because it is a known sensitizer of DPA and its derivatives,[25] and was readily synthesized, with an oleic acid capping ligand, using a previously published procedure.[41] The reaction was monitored with UV−vis absorption spectroscopy, and the QD size was controlled via reaction quenching time in order to maximize absorption at 532 nm to coincide with the frequency doubled Nd:YAG laser excitation line (Figure 2b). From the crossing point between absorption and emission (Figure S1), an E_{0-0} of 2.3 eV was calculated and corresponds to a CdSe QD diameter of ∼2.7 nm.[45]

The multilayer films were prepared using a stepwise soaking procedure (Figure 2a) by first submerging the 4 μm thick nanocrystalline TiO_2 films in a 200 μM solution of **A** in DMSO, followed by a 50 μM solution of **QD** in DCM (Figure S2). The as-synthesized QDs are functionalized with an oleic acid capping ligand.[41] During bilayer formation there is likely ligand exchange at the site of **A** binding, but we anticipate that a majority of the oleic acid capping ligand is retained in the film. This is worth noting as the alkyl capping ligand may serve as a hindrance toward electron transfer from the redox mediator in the electrolyte solution (*vida infra*). In line with previous reports,[46] minimal **QD** adsorption on TiO_2 was

DOI: 10.1021/acsaem.9b01765
ACS Appl. Energy Mater. 2020, 3, 29−37

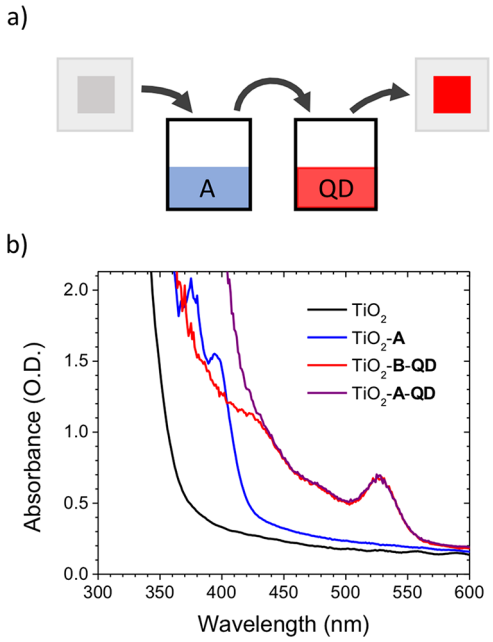

Figure 2. (a) Stepwise soaking procedure and (b) UV−vis absorption spectra of TiO_2, monolayer, and bilayer films.

observed in the absence of a surface bound phosphonate molecule (Figure S3).

As can be seen in Figure 2b, the multilayer assembly is the summed absorption of the constitute components. From the deconvoluted absorption spectra, surface coverages of 127 nmol cm^{-2} and 9 nmol cm^{-2} were obtained for **A** and **QD**, respectively, corresponding to an acceptor to sensitizer ratio of ∼15:1. On a per sensitizer basis, the QD loading is notably lower than our previously reported TiO_2-**A**-Zn-**PtP** (**PtP** = Pt(II)tetrakis(4-carboxyphenyl)porphyrin) multilayer films (3:1) at similar **A** surface coverages.[20] Similar decreased loading has been observed in QD-based dye-sensitized solar cells and is attributed to the relatively large size of the quantum dots hindering diffusion of the sensitizer within the pores of the mesoporous metal oxide film.[46] Attempts to increase pore diameters and QD loadings via changing the TiO_2 preparation procedure (i.e., polymer concentration and autoclave temperature)[47] were moderately successful (Figure S4) but only resulted in a maximum surface loading ratio of ∼15:1. The use of nanorods,[48] inverse opals,[49] or other metal oxide architectures may be necessary to increase QD loadings and maximize light harvesting efficiencies.

3.2. Photovoltaic Characterization. The multilayer films were incorporated into a sandwich solar cell architecture with the TiO_2-dye and Pt on FTO glass as the anode and cathode, respectively, with a 0.2 M/0.02 M Co^{II}/Co^{III} tris(1,10-phenanthroline) redox mediator (Figure 1). $Co^{II/III}(phen)_3$ was chosen as a redox mediator because of previous success in integrated TTA-UC solar cells,[21] and the more traditional dye-sensitized solar cell mediator, I_3^-/I^-, is known to react with CdSe QDs.[50,51] The photoanodes of interest were the **A**-**QD** bilayer (TiO_2-**A**-**QD**) as well as the anthracene only (TiO_2-**A**) and the **QD** only (TiO_2-**B**-**QD**) control films. The latter sample contains the photophysical and electrochemically inert triphenyl-4,4′-diphosphonic acid bridging molecule (**B**) that has a similar structure and binding groups to those of **A** but without concerns of light absorption or energy/electron transfer to **B**.[42]

The short circuit photocurrent density (J_{sc}) with respect to time under solar irradiance (AM1.5) can be seen in Figure 3. A

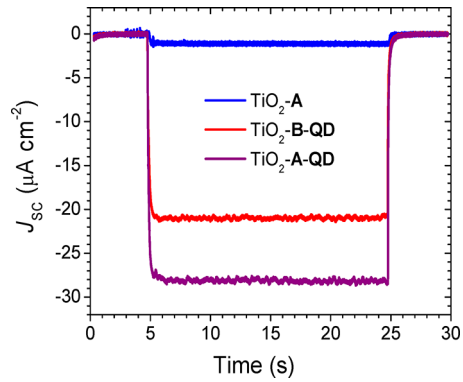

Figure 3. Amperometric *i-t* curves under AM1.5 solar irradiation passed through a 455 nm long pass filter (V = 0 V; light on at 5 s, light off at 25 s).

455 nm long pass filter was used to selectively monitor photocurrent generation in the absence of direct excitation and electron injection from ^{1}**A***. The less than 1 μA cm^{-2} photocurrent from TiO_2-**A** under these conditions suggests that the contribution from direct excitation of **A** is negligible. In contrast, the TiO_2-**A**-**QD** device generates 29 μA cm^{-2} photocurrent under 1 sun intensities. Despite having the same absorption cross-section as the TiO_2-**A** and TiO_2-**B**-**QD**, the J_{sc} for the TiO_2-**A**-**QD** device is ∼1.4 times the sum of its parts, suggesting an enhanced photocurrent generation mechanism. In line with our previous bilayer devices,[21,42] we tentatively assign this mechanism as the excitation of **QD**, energy transfer from **QD*** to **A**, triplet−triplet annihilation between two adjacent ^{3}**A***, and, finally, electron injection from the ^{1}**A*** state (Figure 1). With that said, it is important to note that the 21 μA cm^{-2} for TiO_2-**B**-**QD** suggests that, following excitation, **QD*** can directly inject electrons into the conduction band of TiO_2.

The incident photon-to-current efficiency (IPCE) and absorptance spectrum for a TiO_2-**A**-**QD** device can be seen in Figure 4. The low energy feature of the IPCE spectrum directly coincides with the ∼530 nm transition of the **QD**, indicating that it is involved in the photocurrent generation pathway. When overlaying the 530 nm feature of the spectra in Figure 4, at <450 nm there is a notable deviation between the

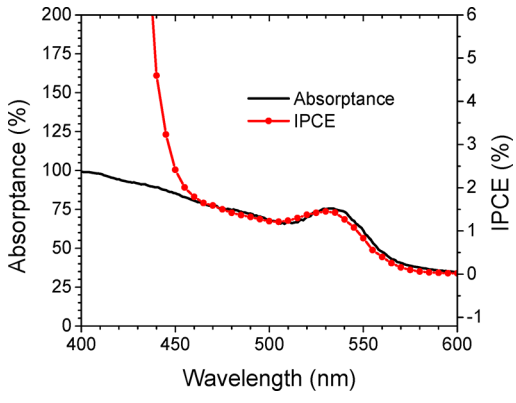

Figure 4. IPCE and absorptance spectrum for a TiO_2-**A**-**QD** integrated TTA-UC solar cell.

DOI: 10.1021/acsaem.9b01765
ACS Appl. Energy Mater. 2020, 3, 29−37

absorptance and IPCE. For a solar cell where every absorbed photon is harvested with the same efficiency, one would expect direct agreement between the IPCE and absorptance spectrum.[52] For the TiO_2-**A**-**QD** device, the deviation can be rationalized by the inherently lower efficiency of TTA-UC (Φ_{max} < 50%) than direct excitation and electron injection (Φ_{max} up to 100%).[53] That is, below 450 nm, photocurrent generation from direct excitation and injection from ^{1}**A*** is more efficient than at >450 nm where **QD** excitation is followed by energy transfer, TTA, and electron injection.

To gain additional insights into the photocurrent generation mechanism we monitored the J_{sc} for TiO_2-**B**-**QD** and TiO_2-**A**-**QD** with respect to excitation intensity, and the log−log plot of the results are shown in Figure 5. For the QD only control

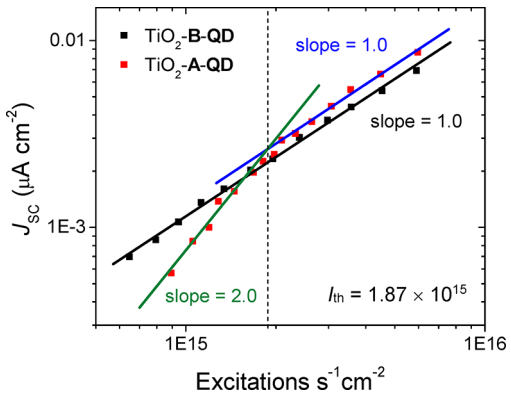

Figure 5. J_{sc} with respect to excitation rate (λ_{ex} = 532 nm).

(TiO_2-**B**-**QD**) there is a linear response (slope = 1.0) that is consistent with excitation and direct electron transfer from **QD*** to TiO_2. In contrast, for the TiO_2-**A**-**QD** bilayer there is a transition from quadratic (slope = 2.0) to linear (slope = 1.0) dependence at low and high intensity excitation, respectively. This quadratic-to-linear transition is symptomatic of a TTA-UC photocurrent generation mechanism.[54,55] Additionally, the sharp J_{sc} decrease and slope of 2.0 at low excitation intensities suggests that the photocurrent contribution from direct **QD*** to TiO_2 electron transfer is negligible. If **QD*** to TiO_2 electron transfer were a major contributor to the TiO_2-**A**-**QD** device performance, we would expect (1) a photocurrent comparable to the TiO_2-**B**-**QD** device and (2) a subquadratic response in the low intensity regime. The lack of these observations indicates that in the bilayer **QD*** to **A** energy transfer is faster than **QD*** to TiO_2 electron injection. Unfortunately, one way to interpret this result is that at low intensities the incorporation of an acceptor molecule serves as an energy trap for a less efficient photocurrent generation pathway. Nonetheless, in the linear regime, TTA-UC gives a photocurrent enhancement.

The crossover point between quadratic and linear regimes (i.e., the I_{th} value) is the minimum excitation intensity necessary for TTA-UC to reach its maximum efficiency in a given system.[54,55] For the TiO_2-**A**-**QD** device under 532 nm excitation, the I_{th} value is 0.9 mW cm^{-2}, which is below AM1.5 solar flux integrated from 480 to 535 nm (6 mW cm^{-2}) and is on par with some of the lowest I_{th} values reported to date.[56,57] To facilitate comparisons between different sensitizer systems, excitation wavelengths, and absorption profiles, we also calculated the I_{th} value in excitations per second (photons s^{-1} cm^{-2} × absorptance) to be 1.87 × 10^{15} ex s^{-1} cm^{-2}.

Given their surprising similarity but also notable differences, it is worth comparing the **QD** sensitized device reported here (TiO_2-**A**-**QD**) to our prototypical **PtP** sensitized device (TiO_2-**A**-Zn-**PtP**).[21] Despite the **QD** films having significantly lower sensitizer loadings (15:1 vs 3:1, *vida supra*), both films exhibit similar low light absorption (~0.7 O.D.) which can be attributed to the ~4-fold larger extinction coefficient for **QD** (6.9 × 10^4 M^{-1} cm^{-1} at 532 nm) than that of **PtP** (1.7 × 10^3 M^{-1} cm^{-1} at 532 nm).[15] Remarkably, when expressed in excitations per second (ex s^{-1}), both the **QD** and **PtP** sensitized films have similar I_{th} values of 1.9 × 10^{15} ex s^{-1} cm^{-2} and 2.1 × 10^{15} ex s^{-1} cm^{-2}, respectively.[22] The parameters dictating the I_{th} value are described in eq 1:

$$I_{th} = \frac{1}{\Phi_{ET} \times \alpha(E) \times (\tau_A{}^3)^2 \times \gamma_{TTA}} \quad (1)$$

where $\tau_A{}^3$ is the triplet excited state lifetime of **A**, Φ_{ET} is the **QD*** to **A** ET efficiency, $\alpha(E)$ is the sensitizer absorption cross-section, and γ_{TTA} is the second-order rate constant for TTA.[55] Because the films have similar $\alpha(E)$ and Φ_{ET} (*vida infra*) values, the similarity in the I_{th} value suggests that the choice of sensitizer has minimal influence on $\tau_A{}^3$ or γ_{TTA}. These properties may be entirely dictated by the TiO_2-**A** interface and not by subsequent metal ion or sensitizer layers. In contrast, it has previously been shown that using the same sensitizer but with variations in the surface binding motif of the anthracene monolayer results in an increase or decrease of γ_{TTA} by more than an order of magnitude.[58,59] Collectively, these results indicate that if one could increase the **QD** loading and select the appropriate **A** monolayer, then a lower I_{th} value and higher photocurrent could be achieved.

Despite the similarities noted above, the J_{sc} for the TiO_2-**A**-**QD** device (29 μA cm^{-2}) is more than 6-fold lower than for TiO_2-**A**-Zn-**PtP** (185 μA cm^{-2}).[21] Since the absorbance and I_{th} values are similar, the dramatically lower photocurrent implies that events after TTA-UC (i.e., back singlet energy transfer, fast charge recombination, and/or slow regeneration) are hindering the total photocurrent generation in the TiO_2-**A**-**QD** device.

3.3. Energy and Electron Transfer Dynamics. To gain insights into the **QD*** to **A** energy transfer process we performed steady-state and time-resolved emission measurements on TiO_2-**B**-**QD** and TiO_2-**A**-**QD** films, and the results can be seen in Figure 6. In both films, emission from **QD** is observed from 500 to 600 nm, indicating that, unlike dyes directly bound to the surface,[60] **QD*** to TiO_2 electron transfer is not an efficient excited state quenching process. Also, in comparison to TiO_2-**B**-**QD**, there is a nearly 8-fold decrease in emission intensity from the TiO_2-**A**-**QD** film. If we assume that the only additional quenching mechanism introduced by **A** is energy transfer, then quenching equates to an ~85% **QD*** to **A** energy transfer efficiency (Φ_{ET}).

As can be seen in the time-resolved emission data (inset Figure 6), there is a corresponding decrease in QD emission lifetime from TiO_2-**B**-QD (18 ns) to TiO_2-**A**-QD (10 ns). Again, assuming the decrease in emission lifetime is due to **QD*** to **A** energy transfer, then an energy transfer rate (k_{ET}) of 4 × 10^7 s^{-1} can be calculated using eq 2

$$k_{ET} = \frac{1}{\tau_{A-QD}} - \frac{1}{\tau_{B-QD}} \quad (2)$$

DOI: 10.1021/acsaem.9b01765
ACS Appl. Energy Mater. 2020, 3, 29−37

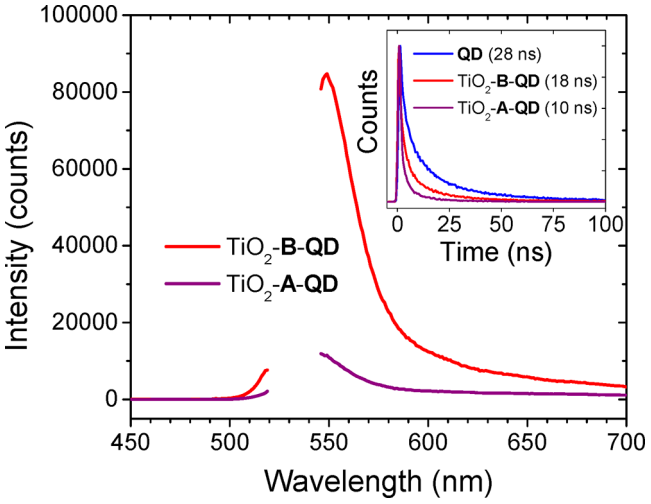

Figure 6. Steady-state emission for TiO_2-**B-QD** and TiO_2-**A-QD** films in MeCN (λ_{ex} = 532 nm; data from 520 to 540 nm were omitted due to scatter from the excitation source). Inset: time-resolved decay traces for **QD** in toluene and both films in MeCN (λ_{ex} = 445 nm, λ_{em} = 545 nm).

where τ_{A-QD} and τ_{B-QD} are the emission lifetimes for TiO_2-**A-QD** and TiO_2-**B-QD**, respectively.[42] Likewise, an ET efficiency (Φ_{ET}) of 45% can be estimated using eq 3.

$$\Phi_{ET} = 1 - \frac{\tau_{A-QD}}{\tau_{B-QD}} \quad (3)$$

The discrepancy between the Φ_{ET} from steady-state (85%) and time-resolved (45%) emission measurements suggests that there are subnanosecond quenching dynamics occurring within our instrument response function (~1 ns) and that 4×10^7 s^{-1} is a low-end estimate of k_{ET}. This time-resolution limitation suggests that steady-state emission provides a more accurate representation of the true energy transfer yield but with the disclaimer that the sample to sample variation for steady-state emission is much larger (5−10 percentage points) due to light scatter and film inhomogeneities. Ultimately, directly measuring ultrafast excited state dynamics will be key to determining the true energy transfer rate and yield.

As a side note, there is a decrease in emission lifetime from the **QD** in solution (τ_{QD} = 28 ns) to in the TiO_2-**B-QD** bilayer film (18 ns). Assuming the decrease in emission lifetime is exclusively due to electron transfer quenching by TiO_2, then a low-end estimate of the electron injection rate (k_{inj}) of 2×10^7 s^{-1} can be calculated using eq 4.[38,61]

$$k_{inj} = \frac{1}{\tau_{B-QD}} - \frac{1}{\tau_{QD}} \quad (4)$$

In agreement with the conclusion from the intensity dependent data in Figure 5, the two-times larger k_{ET} than k_{inj} suggests that direct **QD*** to TiO_2 electron injection has minimal contribution to the photocurrent generation from the TiO_2-**A-QD** film.

In the proposed mechanism, **QD*** to **A** energy transfer is followed by TTA between two ^{3}**A*** and electron injection from ^{1}**A*** into TiO_2, resulting in the formation of $\mathbf{A}^+$. To follow the fate of the cation, we turned to transient absorption (TA) spectroscopy, and the results can be seen in Figure 7a. For the films without **QD** (TiO_2-**A**), direct excitation of **A** at 360 nm is followed by electron injection from ^{1}**A*** into TiO_2 and with $\mathbf{A}^+$

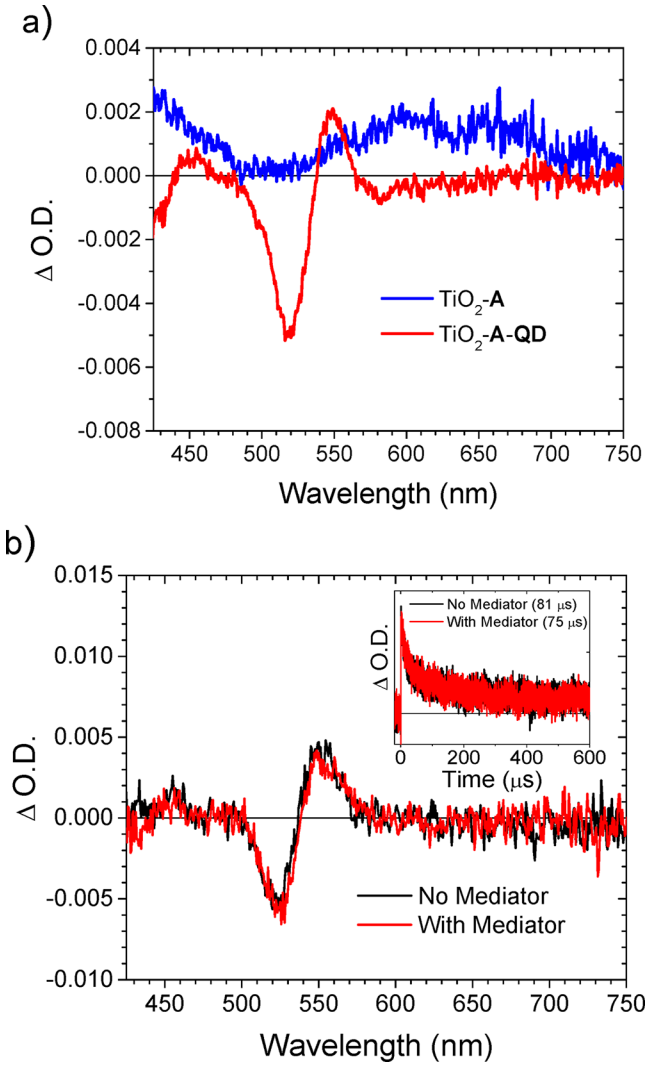

Figure 7. Transient absorption spectra of (a) TiO_2-**A** and TiO_2-**A-QD** in MeCN at 10 ns after 360 nm excitation. (b) TiO_2-**B-QD** films with and without $Co^{II/III}(phen)_3$ redox mediator in MeCN at 100 μs after 455 nm excitation (inset: kinetic decay trace of the same films at 545 nm).

formation indicated by the positive absorption feature from 500 to 750 nm.[42] In contrast, the TA spectrum for TiO_2-**A-QD**, excited at 360 nm for preferential excitation of **A**, has distinct spectral features including a bleach from 485 to 530 nm and positive absorption from 530 to 560 nm. These spectral features agree with those found for TiO_2-**B-QD** excited at 455 nm (Figure 7b; i.e., $\mathbf{QD}^+$ formation from direct **QD*** to TiO_2 electron transfer) as well as the previous reported CdSe cation ($\mathbf{QD}^+$).[32] The absence of any spectral features for $\mathbf{A}^+$ at 10 ns indicates that **QD** to $\mathbf{A}^+$ electron transfer (k_{eT}) is faster than 1×10^8 s^{-1}. Interestingly, this result is in contrast to the anthracene−CdSe system reported by Shan et al., where no spectral features for QD^+ (i.e., −ΔA from 485 to 530 nm and +ΔA from 530 to 560 nm) were observed (see Figure 3 from ref 32).[32] While the energetics are similar to the assembly reported here, the primary difference is their use of a carboxylated anthracene dye that may slow or hinder electron transfer for reasons unknown to us.

Following $\mathbf{QD}^+$ formation, electron transfer from the mediator in solution to the oxidized dye is a key step in

DOI: 10.1021/acsaem.9b01765
ACS Appl. Energy Mater. 2020, 3, 29−37

generating sustained photocurrent (i.e., regeneration or k_{regen} in Figure 1). To monitor the **QD**$^+$ regeneration process we performed transient absorption on TiO_2-**B**-**QD** films with and without the redox mediator solution, and the results can be seen in Figure 7b. As noted above, for TiO_2-**B**-**QD** under direct **QD** excitation, spectral features consistent with **QD**$^+$ are observed. These features persist for >500 μs but gradually return to the baseline due to recombination between **QD**$^+$ and the previously injected electron in TiO_2. Interestingly, upon the addition of $Co^{II/III}(phen)_3$ redox mediator there were no changes in the spectral features and minimal changes in the **QD**$^+$ lifetime, indicating that k_{regen} is a slow process ($<1 \times 10^4$ s^{-1}) likely due to either slow diffusion of the mediator within the pores or slow Co^{II} to **QD**$^+$ electron transfer kinetics. Similar slow regenerate kinetics by cobalt tris-polypyridyl mediators have been observed in CdSe QD-dye sensitized solar cells.[62] Presumably the oleic acid capping group inhibits close contact between **QD**$^+$ and the Co^{II} mediator. Regardless of the cause, this slow regeneration is likely responsible, at least in part, for the low photocurrent from the TiO_2-**A**-**QD** device as compared to our previously reported TiO_2-**A**-Zn-**PtP** system.

In addition to serving as a productive electron donor, we have previously shown that the $Co^{II/III}$ mediators can also act as a quencher for triplet excited states in the TTA-UC scheme.[21,63,64] To probe the possible quenching of the **QD** excited state by the mediator, we performed steady-state and time-resolved emission on TiO_2-**B**-**QD** films with and without $Co^{II/II}(phen)_3$, and the results can be seen in Figure 8. There is a nearly 10-fold decrease in emission intensity and 2-fold decrease in excited state lifetime for the **QD** upon the addition of $Co^{II/II}(phen)_3$. Using slight variations of eqs 2 and 3, 8×10^7 s^{-1} and ~60%, were determined as the rate and efficiency for quenching of **QD*** by $Co^{II/III}(phen)_3$, respectively. This observation indicates that excited state quenching of **QD*** by $Co^{II/III}(phen)_3$ is an additional competitive quenching pathway that can hinder photocurrent generation in the device.

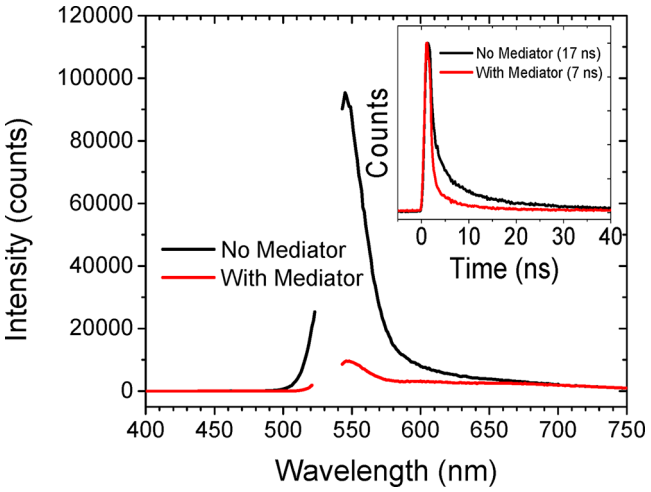

Figure 8. Emission spectra of TiO_2-**B**-**QD** films in MeCN with and without 0.2/0.02 M $Co^{II/II}(phen)_3$ (λ_{ex} = 532 nm). Inset: time-resolved decay traces for **QD*** with and without mediator (λ_{ex} = 445 nm, λ_{em} = 545 nm).

3.4. QD Size Dependence. One distinct advantage of QDs over molecular sensitizers is that their energetics can readily be tuned by varying the size of the QDs. With this in mind we generated three different sizes of CdSe QDs (2.3, 2.7, and 3.1 nm) by varying the reaction quenching times (see the Supporting Information for details). The photophysical properties and their performance in the TiO_2-**A**-**QD** bilayer were measured, and the results are summarized in Table 1.

As the size increases, the surface coverage of **QD** in the TiO_2-**A**-**QD** bilayer decreases from 17.0 to 8.7 to 7.3 nmol cm^{-2} which is perhaps not surprising given the pore size limitations mentioned above. However, in terms of light harvesting efficiency, the decreased surface coverage is partially offset by the increased extinction coefficient and lower energy absorption onset of the larger **QD**s (Figure 9a). Interestingly, the energy transfer efficiencies were reasonably similar (27–44%) with no obvious correlation between Φ_{ET} and **QD** size. In all cases **QD** (>2.2 eV) to **A** (~1.8 eV)[36] energy transfer is favorable by >400 meV and any decrease in driving force for the larger particles is likely offset by the increased excited state lifetime for the larger **QD** (Table S1). It is worth noting that the energy transfer efficiency is limited by the spatial separation (i.e., the phenyl phosphonate) between the QD and the anthracene as was previously observed by Li et al.[65]

When incorporated into the device, all three TiO_2-**A**-**QD** films generate >20 μA cm^{-2} and exhibit quadratic to linear intensity dependence consistent with a TTA-UC mechanism (Figure 9b).[54,55] Correcting for absorption differences at the laser excitation wavelength, there was a trend of increasing I_{th} value with particle size with a more than 2-fold difference between the 2.3 nm (1.5×10^{15} ex s^{-1} cm^{-2}) and the 3.1 nm (3.8×10^{15} ex s^{-1} cm^{-2}) **QD** films. If we assume that $\tau_A{}^3$ is the same accross all **A** monolayers, and since the energy transfer yields are similar in both films (~30%), then the 2-fold increase in I_{th} may point to differences in γ_{TTA}. In these films, γ_{TTA} is dictated by both cross surface triplet migration and the rate of TTA between adjacent ^{3}**A***. If TTA is limited by triplet diffusion, then the increase in I_{th} for the films containing larger **QD**s can be rationalized by the more than 2-fold decrease in surface coverage, increased intersensitizer distance, and slowed rate of ^{3}**A*** contact. Direct monitoring and modeling of the ^{3}**A*** random walk hopping rate is necessary to further support this hypothesis.

Table 1. Properties and Device Performance Metrics for TiO_2-A-QD Films Containing QDs of Different Diameters

D (nm)[a]	E_{0-0} (eV)	ε (M^{-1} cm^{-1})[a]	Γ (nmol cm^{-2})	Φ_{ET} (%)	I_{th} (mW cm^{-2})[e]	I_{th} (ex s^{-1} cm^{-2})[e]	J_{sc} (μA cm^{-2})[f]
2.3	2.5	50500[b]	17.0	32	0.8	1.5×10^{15}	20
2.7	2.3	77800[c]	8.7	44	0.9	1.9×10^{15}	29
3.1	2.2	115600[d]	7.3	27	1.7	3.8×10^{15}	23

[a]Calculated from the absorbance according to ref 44, [b]λ_{abs} = 490 nm, [c]λ_{abs} = 527 nm, [d]λ_{abs} = 550 nm, [e]λ_{ex} = 455 nm for the 2.3 nm QDs and λ_{ex} = 532 nm for the 2.7 and 3.1 nm QDs, and [f]under AM1.5 solar flux passed through a 455 nm long pass filter. Photocurrents were reproducible across three independent samples with a standard deviation ±3 μA cm^{-2}.

DOI: 10.1021/acsaem.9b01765
ACS Appl. Energy Mater. 2020, 3, 29–37

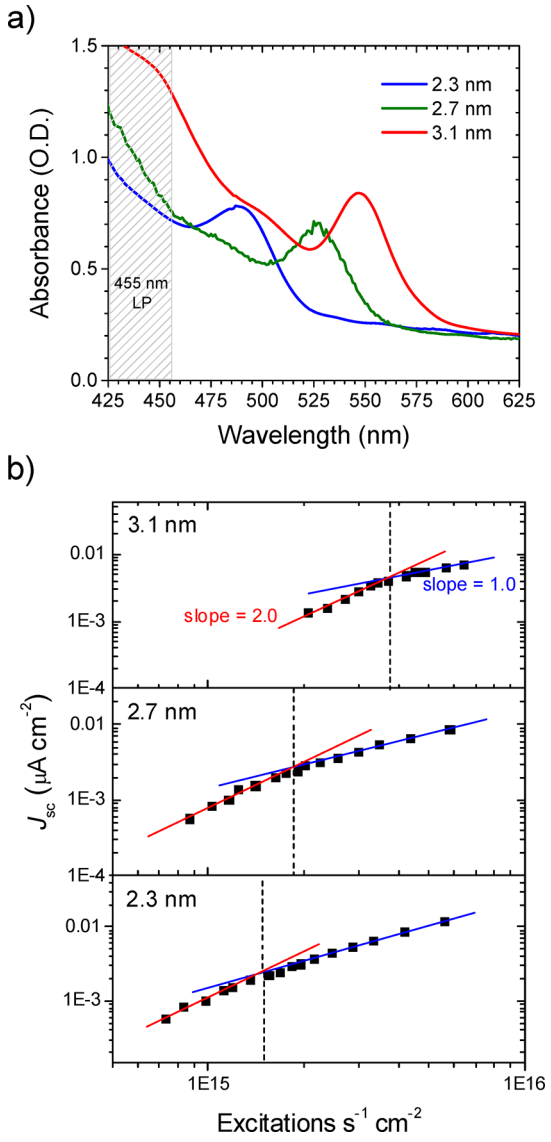

Figure 9. (a) Absorption spectra with light blocked by a 455 nm LP filter (shaded gray) and (b) J_{sc} with respect to excitations s^{-1} cm^{-2} for TiO_2-**A**-**QD** films containing 2.3, 2.7, and 3.1 nm CdSe QDs.

Regardlesses of the differences in I_{th}, all three devices are reaching their maximum efficiency threshold (i.e., the I_{th} value) at <2 mW cm^{-2}, which is below AM1.5 solar flux at the excitation wavelength (>2 mW cm^{-2}).[15] Since they are all operating in the linear regime, have similar energy transfer yields, and have comparable integrated absorption rates (1.44, 1.35, and 1.94 × 10^{28} photons s^{-1} cm^{-2} for 2.3, 2.7, and 3.1 nm **QD** films, respectively), then the similarity in J_{sc} (20−30 μA cm^{-2}) is not surprising. It is, however, worth noting that direct injection from **QD*** in the TiO_2-**B**-**QD** devices was strongly dependent on particle size with a photocurrent of <2 μA cm^{-2} for the 3.1 nm film (Figure S9). This observation agrees with the trend of decreasing conduction band energy (i.e., excited state reduction potential) with increasing size of the **QD**s (Figure S11),[45] and further supports a TTA-UC photocurrent generation mechanism.

4. CONCLUSIONS

CdSe QDs were successfully used as the sensitizer in an integrated TTA-UC solar cell. J_{sc} enhancements greater than 1.4 times the sum of the individual components were achieved using inorganic−organic−inorganic (TiO_2-acceptor-QD) layered photoanodes. The proposed TTA-UC photocurrent generation mechanism (i.e., **QD** excitation, **QD*** to **A** energy transfer, TTA between two ^{3}**A***, and electron injection from ^{1}**A***) was supported by a quadratic to linear photocurrent dependence on excitation intensity. The maximum efficiency onset intensity (i.e., the I_{th} value) was found to be below the solar flux and, in terms of ex s^{-1} cm^{-2} (~2.0 × 10^{15}), was on par with the previously reported molecular sensitized systems despite having a 15-fold lower surface coverage. Regardless of the similarities, the J_{sc} for the QD sensitized device (29 μA cm^{-2}) was more than six times lower than for the previously reported molecular sensitized devices (185 μA cm^{-2}). Time-resolved spectroscopic measurements indicate that less than unity energy transfer yields (~40−80%), slow regeneration kinetics, and competitive QD* quenching by the $Co^{II/III}(phen)_3$ redox mediator are partially responsible for the decreased performance of the QD sensitized device. Regardless, these results demonstrate that QD sensitized upconversion can be harnessed in an integrated TTA-UC solar cell. Increasing QD surface loadings, shifting UC QD-A pairs to the near-IR, increasing energy transfer yields, and speeding up regeneration kinetics are necessary steps to fully realize the potential for QD sensitized TTA-UC solar cells.

■ ASSOCIATED CONTENT

Supporting Information

The Supporting Information is available free of charge on the ACS Publications website at DOI: 10.1021/acsaem.9b01765.

Experimental details, photophysical properties of **QD**, device measurement data, and transient absorption spectra (PDF)

■ AUTHOR INFORMATION

Corresponding Author

*E-mail: hanson@chem.fsu.edu.

ORCID

Drake Beery: 0000-0001-9605-1803
Jonathan P. Wheeler: 0000-0002-8737-0834
Kenneth Hanson: 0000-0001-7219-7808

Notes

The authors declare no competing financial interest.

■ ACKNOWLEDGMENTS

This research was primarily supported by the National Science Foundation (DMR-1752782). Transient absorption measurements were performed on a spectrometer supported by the National Science Foundation (CHE-1531629).

■ REFERENCES

(1) Shockley, W.; Queisser, H. J. Detailed Balance Limit of Efficiency of p-n Junction Solar Cells. *J. Appl. Phys.* **1961**, *32* (3), 510−519.

(2) Ekins-Daukes, N. J.; Schmidt, T. W. A molecular approach to the intermediate band solar cell: The symmetric case. *Appl. Phys. Lett.* **2008**, *93* (6), No. 063507.

(3) Baluschev, S.; Yakutkin, V.; Miteva, T.; Wegner, G.; Roberts, T.; Nelles, G.; Yasuda, A.; Chernov, S.; Aleshchenkov, S.; Cheprakov, A. A general approach for non-coherently excited annihilation up-conversion: transforming the solar-spectrum. *New J. Phys.* **2008**, *10* (1), No. 013007.

DOI: 10.1021/acsaem.9b01765
ACS Appl. Energy Mater. 2020, 3, 29−37

(4) Trupke, T.; Green, M. A.; Würfel, P. Improving solar cell efficiencies by up-conversion of sub-band-gap light. *J. Appl. Phys.* **2002**, *92* (7), 4117−4122.
(5) Singh-Rachford, T. N.; Castellano, F. N. Photon upconversion based on sensitized triplet−triplet annihilation. *Coord. Chem. Rev.* **2010**, *254* (21−22), 2560−2573.
(6) Frazer, L.; Gallaher, J. K.; Schmidt, T. W. Optimizing the Efficiency of Solar Photon Upconversion. *ACS Energy Letters* **2017**, *2* (6), 1346−1354.
(7) Dilbeck, T.; Hanson, K. Molecular Photon Upconversion Solar Cells Using Multilayer Assemblies: Progress and Prospects. *J. Phys. Chem. Lett.* **2018**, *9* (19), 5810−5821.
(8) Cheng, Y. Y.; Fückel, B.; MacQueen, R. W.; Khoury, T.; Clady, R. G. C. R.; Schulze, T. F.; Ekins-Daukes, N. J.; Crossley, M. J.; Stannowski, B.; Lips, K.; Schmidt, T. W. Improving the light-harvesting of amorphous silicon solar cells with photochemical upconversion. *Energy Environ. Sci.* **2012**, *5* (5), 6953−6959.
(9) Schulze, T. F.; Czolk, J.; Cheng, Y.-Y.; Fückel, B.; MacQueen, R. W.; Khoury, T.; Crossley, M. J.; Stannowski, B.; Lips, K.; Lemmer, U.; Colsmann, A.; Schmidt, T. W. Efficiency Enhancement of Organic and Thin-Film Silicon Solar Cells with Photochemical Upconversion. *J. Phys. Chem. C* **2012**, *116* (43), 22794−22801.
(10) Nattestad, A.; Cheng, Y. Y.; MacQueen, R. W.; Schulze, T. F.; Thompson, F. W.; Mozer, A. J.; Fückel, B.; Khoury, T.; Crossley, M. J.; Lips, K.; Wallace, G. G.; Schmidt, T. W. Dye-Sensitized Solar Cell with Integrated Triplet−Triplet Annihilation Upconversion System. *J. Phys. Chem. Lett.* **2013**, *4* (12), 2073−2078.
(11) Lin, Y. L.; Koch, M.; Brigeman, A. N.; Freeman, D. M. E.; Zhao, L.; Bronstein, H.; Giebink, N. C.; Scholes, G. D.; Rand, B. P. Enhanced sub-bandgap efficiency of a solid-state organic intermediate band solar cell using triplet−triplet annihilation. *Energy Environ. Sci.* **2017**, *10* (6), 1465−1475.
(12) Simpson, C.; Clarke, T. M.; MacQueen, R. W.; Cheng, Y. Y.; Trevitt, A. J.; Mozer, A. J.; Wagner, P.; Schmidt, T. W.; Nattestad, A. An intermediate band dye-sensitised solar cell using triplet-triplet annihilation. *Phys. Chem. Chem. Phys.* **2015**, *17* (38), 24826−24830.
(13) Lissau, J. S.; Gardner, J. M.; Morandeira, A. Photon Upconversion on Dye-Sensitized Nanostructured ZrO2 Films. *J. Phys. Chem. C* **2011**, *115* (46), 23226−23232.
(14) Lissau, J. S.; Nauroozi, D.; Santoni, M.-P.; Ott, S.; Gardner, J. M.; Morandeira, A. Anchoring Energy Acceptors to Nanostructured ZrO2 Enhances Photon Upconversion by Sensitized Triplet−Triplet Annihilation Under Simulated Solar Flux. *J. Phys. Chem. C* **2013**, *117* (28), 14493−14501.
(15) Hill, S. P.; Dilbeck, T.; Baduell, E.; Hanson, K. Integrated Photon Upconversion Solar Cell via Molecular Self-Assembled Bilayers. *ACS Energy Letters* **2016**, *1* (1), 3−8.
(16) Wang, J. C.; Hill, S. P.; Dilbeck, T.; Ogunsolu, O. O.; Banerjee, T.; Hanson, K. Multimolecular assemblies on high surface area metal oxides and their role in interfacial energy and electron transfer. *Chem. Soc. Rev.* **2018**, *47* (1), 104−148.
(17) Morifuji, T.; Takekuma, Y.; Nagata, M. Integrated Photon Upconversion Dye-Sensitized Solar Cell by Co-adsorption with Derivative of Pt−Porphyrin and Anthracene on Mesoporous TiO2. *ACS Omega* **2019**, *4* (6), 11271−11275.
(18) Ahmad, S.; Liu, J.; Gong, C.; Zhao, J.; Sun, L. Photon Up-Conversion via Epitaxial Surface-Supported Metal−Organic Framework Thin Films with Enhanced Photocurrent. *ACS Applied Energy Materials* **2018**, *1* (2), 249−253.
(19) Hanson, K.; Torelli, D. A.; Vannucci, A. K.; Brennaman, M. K.; Luo, H.; Alibabaei, L.; Song, W.; Ashford, D. L.; Norris, M. R.; Glasson, C. R. K.; Concepcion, J. J.; Meyer, T. J. Self-Assembled Bilayer Films of Ruthenium(II)/Polypyridyl Complexes through Layer-by-Layer Deposition on Nanostructured Metal Oxides. *Angew. Chem., Int. Ed.* **2012**, *51* (51), 12782−12785.
(20) Dilbeck, T.; Hill, S. P.; Hanson, K. Harnessing molecular photon upconversion at sub-solar irradiance using dual sensitized self-assembled trilayers. *J. Mater. Chem. A* **2017**, *5* (23), 11652−11660.
(21) Hill, S. P.; Hanson, K. Harnessing Molecular Photon Upconversion in a Solar Cell at Sub-solar Irradiance: Role of the Redox Mediator. *J. Am. Chem. Soc.* **2017**, *139* (32), 10988−10991.
(22) Zhou, Y.; Ruchlin, C.; Robb, A. J.; Hanson, K. Singlet Sensitization-Enhanced Upconversion Solar Cells via Self-Assembled Trilayers. *ACS Energy Letters* **2019**, *4* (6), 1458−1463.
(23) Goldschmidt, J. C.; Fischer, S. Upconversion for Photovoltaics − a Review of Materials, Devices and Concepts for Performance Enhancement. *Adv. Opt. Mater.* **2015**, *3* (4), 510−535.
(24) Simone, B. C. D.; Mazzone, G.; Russo, N.; Sicilia, E.; Toscano, M. Metal Atom Effect on the Photophysical Properties of Mg(II), Zn(II), Cd(II), and Pd(II) Tetraphenylporphyrin Complexes Proposed as Possible Drugs in Photodynamic Therapy. *Molecules* **2017**, *22* (7), 1093.
(25) Garakyaraghi, S.; Castellano, F. N. Nanocrystals for Triplet Sensitization: Molecular Behavior from Quantum-Confined Materials. *Inorg. Chem.* **2018**, *57* (5), 2351−2359.
(26) Mongin, C.; Garakyaraghi, S.; Razgoniaeva, N.; Zamkov, M.; Castellano, F. N. Direct observation of triplet energy transfer from semiconductor nanocrystals. *Science* **2016**, *351* (6271), 369.
(27) Huang, Z.; Li, X.; Mahboub, M.; Hanson, K. M.; Nichols, V. M.; Le, H.; Tang, M. L.; Bardeen, C. J. Hybrid Molecule−Nanocrystal Photon Upconversion Across the Visible and Near-Infrared. *Nano Lett.* **2015**, *15* (8), 5552−5557.
(28) Huang, Z.; Li, X.; Yip, B. D.; Rubalcava, J. M.; Bardeen, C. J.; Tang, M. L. Nanocrystal Size and Quantum Yield in the Upconversion of Green to Violet Light with CdSe and Anthracene Derivatives. *Chem. Mater.* **2015**, *27* (21), 7503−7507.
(29) Mahboub, M.; Huang, Z.; Tang, M. L. Efficient Infrared-to-Visible Upconversion with Subsolar Irradiance. *Nano Lett.* **2016**, *16* (11), 7169−7175.
(30) Ronchi, A.; Brazzo, P.; Sassi, M.; Beverina, L.; Pedrini, J.; Meinardi, F.; Monguzzi, A. Triplet−triplet annihilation based photon up-conversion in hybrid molecule−semiconductor nanocrystal systems. *Phys. Chem. Chem. Phys.* **2019**, *21* (23), 12353−12359.
(31) Okumura, K.; Mase, K.; Yanai, N.; Kimizuka, N. Employing Core-Shell Quantum Dots as Triplet Sensitizers for Photon Upconversion. *Chem. - Eur. J.* **2016**, *22* (23), 7721−7726.
(32) Shan, B.; Li, T.-T.; Brennaman, M. K.; Nayak, A.; Wu, L.; Meyer, T. J. Charge Transfer from Upconverting Nanocrystals to Semiconducting Electrodes: Optimizing Thermodynamic Outputs by Electronic Energy Transfer. *J. Am. Chem. Soc.* **2019**, *141* (1), 463−471.
(33) Mongin, C.; Moroz, P.; Zamkov, M.; Castellano, F. N. Thermally activated delayed photoluminescence from pyrenyl-functionalized CdSe quantum dots. *Nat. Chem.* **2018**, *10*, 225.
(34) Efros, A.; Efros, A. L. Interband Light Absorption in Semiconductor Spheres. *Soviet Physics. Semiconductors* **1982**, *16*, 772−775.
(35) Rossetti, R.; Ellison, J. L.; Gibson, J. M.; Brus, L. E. Size effects in the excited electronic states of small colloidal CdS crystallites. *J. Chem. Phys.* **1984**, *80* (9), 4464−4469.
(36) Hill, S. P.; Banerjee, T.; Dilbeck, T.; Hanson, K. Photon Upconversion and Photocurrent Generation via Self-Assembly at Organic−Inorganic Interfaces. *J. Phys. Chem. Lett.* **2015**, *6* (22), 4510−4517.
(37) Lo, C.-Y.; Chen, C.-H.; Tsai, T. W. T.; Zhang, L.; Lim, T.-S.; Fann, W.; Chan, J. C. C.; Luh, T.-Y. Efficient Energy and Electron Transfer between Donor and Acceptor Chromophores in Aluminophosphate Hybrid Materials. *J. Chin. Chem. Soc.* **2010**, *57* (3B), 539−546.
(38) Wang, J. C.; Murphy, I. A.; Hanson, K. Modulating Electron Transfer Dynamics at Dye−Semiconductor Interfaces via Self-Assembled Bilayers. *J. Phys. Chem. C* **2015**, *119* (7), 3502−3508.
(39) Feldt, S. M.; Gibson, E. A.; Gabrielsson, E.; Sun, L.; Boschloo, G.; Hagfeldt, A. Design of Organic Dyes and Cobalt Polypyridine Redox Mediators for High-Efficiency Dye-Sensitized Solar Cells. *J. Am. Chem. Soc.* **2010**, *132* (46), 16714−16724.

DOI: 10.1021/acsaem.9b01765
ACS Appl. Energy Mater. 2020, 3, 29−37

(40) Lee, S.-H. A.; Abrams, N. M.; Hoertz, P. G.; Barber, G. D.; Halaoui, L. I.; Mallouk, T. E. Coupling of Titania Inverse Opals to Nanocrystalline Titania Layers in Dye-Sensitized Solar Cells. *J. Phys. Chem. B* **2008**, *112* (46), 14415−14421.
(41) Knauf, R. R.; Lennox, J. C.; Dempsey, J. L. Quantifying Ligand Exchange Reactions at CdSe Nanocrystal Surfaces. *Chem. Mater.* **2016**, *28* (13), 4762−4770.
(42) Dilbeck, T.; Wang, J. C.; Zhou, Y.; Olsson, A.; Sykora, M.; Hanson, K. Elucidating the Energy- and Electron-Transfer Dynamics of Photon Upconversion in Self-Assembled Bilayers. *J. Phys. Chem. C* **2017**, *121* (36), 19690−19698.
(43) Gallagher, L. A.; Serron, S. A.; Wen, X.; Hornstein, B. J.; Dattelbaum, D. M.; Schoonover, J. R.; Meyer, T. J. Photoelectrochemistry on RuII-2,2′-bipyridine-phosphonate-Derivatized TiO2 with the I3-/I- and Quinone/Hydroquinone Relays. Design of Photoelectrochemical Synthesis Cells. *Inorg. Chem.* **2005**, *44* (6), 2089−2097.
(44) Hanson, K.; Brennaman, M. K.; Luo, H.; Glasson, C. R. K.; Concepcion, J. J.; Song, W.; Meyer, T. J. Photostability of Phosphonate-Derivatized, RuII Polypyridyl Complexes on Metal Oxide Surfaces. *ACS Appl. Mater. Interfaces* **2012**, *4* (3), 1462−1469.
(45) Yu, W. W.; Qu, L.; Guo, W.; Peng, X. Experimental Determination of the Extinction Coefficient of CdTe, CdSe, and CdS Nanocrystals. *Chem. Mater.* **2003**, *15* (14), 2854−2860.
(46) Hines, D. A.; Kamat, P. V. Recent Advances in Quantum Dot Surface Chemistry. *ACS Appl. Mater. Interfaces* **2014**, *6* (5), 3041−3057.
(47) Barbé, C. J.; Arendse, F.; Comte, P.; Jirousek, M.; Lenzmann, F.; Shklover, V.; Grätzel, M. Nanocrystalline Titanium Oxide Electrodes for Photovoltaic Applications. *J. Am. Ceram. Soc.* **1997**, *80* (12), 3157−3171.
(48) Lai, Y.; Lin, Z.; Zheng, D.; Chi, L.; Du, R.; Lin, C. CdSe/CdS quantum dots co-sensitized TiO2 nanotube array photoelectrode for highly efficient solar cells. *Electrochim. Acta* **2012**, *79*, 175−181.
(49) Diguna, L. J.; Shen, Q.; Kobayashi, J.; Toyoda, T. High efficiency of CdSe quantum-dot-sensitized TiO2 inverse opal solar cells. *Appl. Phys. Lett.* **2007**, *91* (2), No. 023116.
(50) Vogel, R.; Hoyer, P.; Weller, H. Quantum-Sized PbS, CdS, Ag2S, Sb2S3, and Bi2S3 Particles as Sensitizers for Various Nanoporous Wide-Bandgap Semiconductors. *J. Phys. Chem.* **1994**, *98* (12), 3183−3188.
(51) Nakatani, K.; Matsudaira, S.; Tsubomura, H. Photoanodic Behavior of n-type Cadmium Sulfide in Acetonitrile Solutions Containing Iodide Ion. *J. Electrochem. Soc.* **1978**, *125* (3), 406−409.
(52) Sharma, K.; Sharma, V.; Sharma, S. S. Dye-Sensitized Solar Cells: Fundamentals and Current Status. *Nanoscale Res. Lett.* **2018**, *13* (1), 381.
(53) Listorti, A.; O'Regan, B.; Durrant, J. R. Electron Transfer Dynamics in Dye-Sensitized Solar Cells. *Chem. Mater.* **2011**, *23* (15), 3381−3399.
(54) Haefele, A.; Blumhoff, J.; Khnayzer, R. S.; Castellano, F. N. Getting to the (Square) Root of the Problem: How to Make Noncoherent Pumped Upconversion Linear. *J. Phys. Chem. Lett.* **2012**, *3* (3), 299−303.
(55) Monguzzi, A.; Mezyk, J.; Scotognella, F.; Tubino, R.; Meinardi, F. Upconversion-induced fluorescence in multicomponent systems: Steady-state excitation power threshold. *Phys. Rev. B: Condens. Matter Mater. Phys.* **2008**, *78* (19), 195112.
(56) Gray, V.; Moth-Poulsen, K.; Albinsson, B.; Abrahamsson, M. Towards efficient solid-state triplet−triplet annihilation based photon upconversion: Supramolecular, macromolecular and self-assembled systems. *Coord. Chem. Rev.* **2018**, *362*, 54−71.
(57) Yanai, N.; Kimizuka, N. Recent emergence of photon upconversion based on triplet energy migration in molecular assemblies. *Chem. Commun.* **2016**, *52* (31), 5354−5370.
(58) Zhou, Y.; Ayad, S.; Ruchlin, C.; Posey, V.; Hill, S. P.; Wu, Q.; Hanson, K. Examining the role of acceptor molecule structure in self-assembled bilayers: surface loading, stability, energy transfer, and upconverted emission. *Phys. Chem. Chem. Phys.* **2018**, *20* (31), 20513−20524.
(59) Zhou, Y.; Hill, S. P.; Hanson, K. Influence of meta- and para-phosphonated diphenylanthracene on photon upconversion in self-assembled bilayers. *J. Photonics Energy* **2018**, *8* (2), 1−11.
(60) Ardo, S.; Meyer, G. J. Photodriven heterogeneous charge transfer with transition-metal compounds anchored to TiO2 semiconductor surfaces. *Chem. Soc. Rev.* **2009**, *38* (1), 115−164.
(61) Wang, J. C.; Violette, K.; Ogunsolu, O. O.; Cekli, S.; Lambers, E.; Fares, H. M.; Hanson, K. Self-Assembled Bilayers on Nanocrystalline Metal Oxides: Exploring the Non-Innocent Nature of the Linking Ions. *Langmuir* **2017**, *33* (38), 9609−9619.
(62) Xie, Y.; Baillargeon, J.; Hamann, T. W. Kinetics of Regeneration and Recombination Reactions in Dye-Sensitized Solar Cells Employing Cobalt Redox Shuttles. *J. Phys. Chem. C* **2015**, *119* (50), 28155−28166.
(63) Ohno, T.; Kato, S. Electron-transfer reactions of excited phthalocyanines: spin restriction on reaction rate of electron transfer and energy transfer to cobalt compounds. *J. Phys. Chem.* **1984**, *88* (8), 1670−1674.
(64) Porter, G.; Wright, M. R. Modes of energy transfer from excited and unstable ionized states. Intramolecular and intermolecular energy conversion involving change of multiplicity. *Discuss. Faraday Soc.* **1959**, *27* (0), 18−27.
(65) Li, X.; Huang, Z.; Zavala, R.; Tang, M. L. Distance-Dependent Triplet Energy Transfer between CdSe Nanocrystals and Surface Bound Anthracene. *J. Phys. Chem. Lett.* **2016**, *7* (11), 1955−1959.

DOI: 10.1021/acsaem.9b01765
ACS Appl. Energy Mater. 2020, 3, 29−37